LANGMUIR

Article

pubs.acs.org/Langmuir

Structural Features of PbS Nanocube Monolayers upon Treatment with Mono- and Dicarboxylic Acids and Thiols at a Liquid−Air Interface

Martin R. McPhail,[†] Gavin P. Campbell,[‡] Michael J. Bedzyk,[‡,§] and Emily A. Weiss*[,†,‡]

[†]Department of Chemistry, [‡]Department of Materials Science and Engineering, and [§]Department of Physics and Astronomy, Northwestern University, Evanston, Illinois 60208-3113, United States

Supporting Information

ABSTRACT: This paper describes the ordering of PbS nanocubes (NCs) within free-standing monolayers (suspended on acetonitrile), upon exchanging the native oleate ligands for a series of thiolate and carboxylate ligands at the liquid−air interface. Treatment with either carboxylic acids or thiols effectively decreases the inter-NC separation of nearest-neighbor particles without etching the NC surface. Dicarboxylic acids and dithiols bridge neighboring NCs with an interparticle separation that is consistent with fully extended, bridging ligands. Monocarboxylic acids and monothiols separate NCs by an amount governed by their length, with long-chain ligands showing significant intercalation. ^{1}H NMR spectroscopy shows carboxylic acids are more effective at replacing the native oleate than are thiols, which we ascribe to the lower pK_a values of carboxylic acids. The fast exchange that occurs upon treatment with monocarboxylic acids kinetically traps the clusters of particles in nonclosed packed geometries, so monolayers treated with monocarboxylic acids are, on average, less ordered than those treated with monothiols. *Ex situ* electron microscopy and grazing incidence small-angle X-ray scattering (GISAXS) analyses of deposited films on Si/SiO_2 substrates show that NCs exchanged with nonbridging ligands pack more efficiently at long length scales than do NCs exchanged with bridging ligands, due primarily to the creation of defects within the NC lattice in response to the rigidity of the bridging ligand.

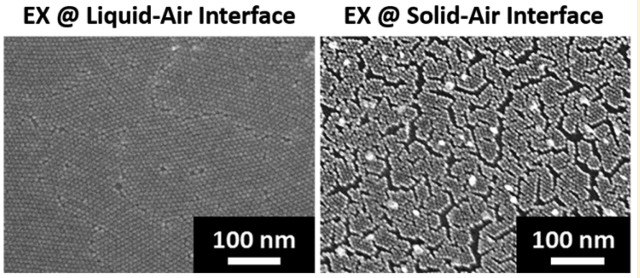

INTRODUCTION

This paper describes the changes in the structure of two-dimensional lead sulfide nanocube (PbS NC) arrays following exchange of the native oleate ligands for a series of mono- and dicarboxylate or -thiolate ligands at a liquid−air interface. As-synthesized NCs are typically coated by a shell of coordinating ligands with long hydrocarbon tails that provide solubility and surface stability. Exchange of these ligands for shorter and/or more electrically conductive ligands is one strategy for improving the rates of interparticle charge and energy transfer. Carrier mobilities in multilayer NC films have been improved by several orders of magnitude through the exchange of oleate or octylphosphonate ligands for 1,2-ethanedithiol,[1] formic acid,[2,3] oxalic acid,[3] thiocyanate,[4] halides,[5] metal sulfides,[6] and hydrazine.[7] These ligand exchanges are performed after NC deposition on a substrate because very short or cross-linking ligands cause aggregation and precipitation of the colloids and an inhomogeneously deposited film. Ligand exchange of the solid-state film is also in some cases problematic because local contractions of the film lead to complete separation of domains that hinder conductivity, especially of single monolayers where only intralayer percolation pathways are available.[4] Work by Dong et al. demonstrated the feasibility of ligand exchange at a liquid−air interface to prepare conductive monolayers of PbS NCs;[2] exchange at a liquid−air interface allows for more facile reorganization of NCs upon exchange with a shorter surface ligand and produces more compact monolayers than exchange of ligands within solid state films.

In this study, we examine the short- and long-range order of monolayers of PbS NCs (truncated cubic in shape, with an average edge length of 9.7 nm), upon exchange of the native oleate ligands with mono- and dicarboxylic acids and thiols at a liquid−air interface. Ligand shells composed of saturated monocarboxylic acids and monothiols adopt a 60−70% intercalated packing geometry, with the exception of formic acid, which does not intercalate. PbS NCs functionalized with dicarboxylates and dithiolates are spaced by a distance equal to the ligand length, so we conclude that these ligands bridge adjacent NCs; this bridging geometry allows for precise control over nearest-neighbor spacing.[3,8−13] We measure the degree of ligand exchange for each system using quantitative ^{1}H NMR and discuss the degree of order in these films with respect to the relative pK_a values, binding affinities, and conformational flexibilities of the ligands, which determine the ability of the NCs to reorganize into a tightly packed structure.

Received: April 14, 2016
Revised: June 3, 2016
Published: June 13, 2016

DOI: 10.1021/acs.langmuir.6b01444
Langmuir 2016, 32, 6666−6673

Field-emission scanning electron microscopy (FE-SEM) shows that ligand exchange produces two important types of defects: (1) relative rotation of one NC with respect to its nearest neighbors and (2) opening of intradomain gaps. Arrays treated with short monocarboxylic acids are especially prone to type 1 defects because these ligands rapidly exchange with the native ligand while simultaneously increasing the energetic barrier to rotation of the NC. Short dicarboxylic acids and dithiols both exhibit type 2 defects by forming covalent linkages between adjacent NCs that limit the ability of bridged clusters of NCs to reorganize into compact domains. These experiments demonstrate the inherent trade-off between the reduction of inter-NC spacing and the introduction of packing defects.

METHODS

Materials. PbS nanocubes (NCs) were synthesized using lead(II) oxide (99.999% trace metals basis), elemental sulfur flakes (99.998% trace metals basis), 1-octadecene (90% tech. grade), oleic acid (90% tech. grade), and oleylamine (70% tech. grade). Formic acid (≥95% reagent grade), acetic acid (≥99.7% ACS Reagent), propionic acid (≥99.5% ACS reagent), butyric acid (≥99%), hexanoic acid (≥99.5%), oxalic acid (99.999% trace metals basis), succinic acid (≥99.0% ACS Reagent), adipic acid (99%), suberic acid (98%), sebacic acid (99%), dodecanedioic acid (99%), ethanethiol (97%), 1-propanethiol (99%), 1-butanethiol (99%), 1-pentanethiol (98%), 1-hexanethiol (95%), 1,3-propanedithiol (99%), 1,4-butanedithiol (97%), 1,6-hexanedithiol (96%), and 1,8-octanedithiol (≥97%) were used as ligands for PbS NCs. Synthetic reagents and ligands were purchased from Sigma-Aldrich. General laboratory grade acetone, acetonitrile, chloroform, tetrahydrofuran, and hexanes used in the purification, deposition, and ligand exchange of PbS NCs were purchased from B&J BDH Solvents. All reagents and solvents were used as-received without further purification.

PbS NC Synthesis. PbS NCs were synthesized using a method adapted from a report by Li et al.[14] We prepared a stock solution of the sulfur precursor by adding 320 mg of elemental sulfur flakes to 100 mL of dried 1-octadecene at 180 °C and stirring under nitrogen for 5 min, during which time the flakes dissolved completely to form a yellow tinted solution. The solution was cooled to room temperature to form a clear, colorless solution and then transferred to vials for later use. This sulfur stock solution was stable for at least several weeks under ambient atmosphere and temperature. We prepared a reaction mixture of lead(II) oleate by adding 357 mg of lead(II) oxide, 56 mL of 1-octadecene, and 5 mL of oleic acid to a round-bottom flask and heating it to 210 °C while flowing dry nitrogen gas through the vessel to obtain a clear, colorless solution. Immediately prior to sulfur precursor injection, 8 mL of oleylamine was injected to the lead(II) oleate reaction mixture to serve as an *in situ* sulfur reducing agent. Once the temperature had again reached 210 °C, 8 mL of the sulfur precursor was swiftly injected into the reaction solution, which produced an immediate color change in the reaction solution from clear to black. The NCs were allowed to grow for 1 min under heating before the reaction was quenched by decanting into ice-chilled chloroform. The NCs were recovered by centrifugation and washed by redispersing in hexanes and reprecipitating in 10:1 (vol:vol) acetone:hexanes. The final NC product was readily soluble in hexanes, chloroform, and tetrachloroethylene.

PbS NC Monolayer Preparation and Ligand Exchange. We prepared the PbS NC casting suspension by dispersing the dried PbS NC powder in hexanes to a concentration of 4 mg/mL. To create the PbS NC monolayer, we delivered 40 μL of this solution to the edge of a 25-mL, round PTFE crucible containing 2 mL of dried acetonitrile. This produced a growing sheet of PbS NC monolayer that completely covered the subphase surface; monolayer growth was typically completed within 10 s. Ligand exchange of this freestanding sheet was accomplished by injecting 10 μL of a stock ligand solution in tetrahydrofuran via microsyringe into the acetonitrile subphase and allowing the ligand composition to equilibrate for 30 min. The stock ligand solutions were all prepared at a concentration of 3.89 M, except for the dicarboxylic acids, which had to be prepared at a concentration of 3.89 mM due to their low solubility in acetonitrile.

TEM and SEM Imaging. All TEM images were acquired on 400 mesh holey carbon-on-copper TEM grids (Ted Pella). In order to determine particle size, we drop-cast aliquots of the PbS NCs in hexanes onto the TEM grid supported on vacuum filtration paper and imaged using a Hitachi H-8100 TEM operating at 200 kV. To image PbS NC monolayers, we prepared and, if appropriate, ligand-exchanged those monolayers as described above, transferred them onto a grid for HR-TEM imaging or an Si/SiO_2 wafer (cleaned by sonicating in methanol followed by acetone) for FE-SEM imaging, as described above, and dried in a vacuum oven for 30 min at 70 °C and 25 in.Hg. We performed HR-TEM of the NC monolayers using a JEOL JEM-2100 TEM operated at 200 kV and FE-SEM using Hitachi SU8030 and Hitachi S4800-II SEMs operated at 20 kV and 10 μA.

Grazing Incidence Small-Angle X-ray Scattering (GISAXS) Acquisition. GISAXS measurements and analysis were performed on single monolayers of ligand-exchanged PbS NCs on $Si(100)/SiO_2$ substrates, prepared using methods consistent with those used for FE-SEM samples. GISAXS measurements were performed using a Rigaku S-Max 3000 equipped with a Vantec 2000 area detector. A microfocus sealed Cu-anode tube source was followed by a cross multilayer mirror optic to produce 8.04 keV X-rays. The beam was passed through a 200 μm slit with the sample held at grazing incident angle of $\alpha = 0.24°$, which is ∼66% of the critical angle for a pure PbS film. The photon flux of $\sim 10^6$ photons/s allowed interrogation of the first three in-plane NC diffraction peaks.

Near-IR Absorption Spectroscopy. To acquire absorption spectra of the NC monolayers, we deposited them, as described above, onto a glass microscope coverslip precleaned by sonicating in methanol followed by acetone. We removed residual solvent from the deposited film by heating it in a vacuum oven at 70 °C and 25 in.Hg for 30 min. We collected the spectra of the dried films between 1000 and 2500 nm using a Varian Cary 5000 UV−vis−NIR spectrophotometer with a reference to air and baselined with a clean glass coverslip.

^{1}H NMR Spectroscopy. We acquired ^{1}H NMR spectra of an acetonitrile-d_3 subphase following ligand exchange, in order to quantify the yield of oleate displacement from the NC layer into the subphase. ^{1}H NMR spectra were taken in acetonitrile-d_3 using an Ag-500 Bruker Avance III 500 MHz nuclear magnetic resonance spectrometer with a biphenyl internal integration standard. The Supporting Information contains the spectra we integrated for this measurement.

RESULTS AND DISCUSSION

We synthesized oleate-capped PbS NCs with a truncated cubic geometry (Figure 1a) using a hot injection method, as described in the Methods section. The average edge length, extracted from a Gaussian fit to a histogram of 873 NC edge lengths measured by transmission electron microscopy, has a mean value of 9.7 nm with standard deviation of 0.7 nm (Figure 1a, inset). These NCs are useful for structural studies of ligand-exchanged NC monolayers because they are (i) small enough to maintain strong quantum confinement (the Bohr exciton radius of PbS is 20 nm),[15] (ii) large enough to be clearly imaged by field-emission scanning electron microscopy, and (iii) similar in size to those previously used for preparation of flexible field effect transistors and conductive monolayers.[2,4] The anisotropic geometry of these cubic NCs also makes them interesting for a study of packing structures; the 4-fold rotational symmetry of the NCs introduces packing disorder produced by the relative rotation of nearest-neighbor NCs.

The preparation of PbS NC monolayers via self-assembly at a liquid−air interface followed by ligand exchange at this interface was based on previous reports by Dong et al.[2,16]

DOI: 10.1021/acs.langmuir.6b01444
Langmuir 2016, 32, 6666−6673

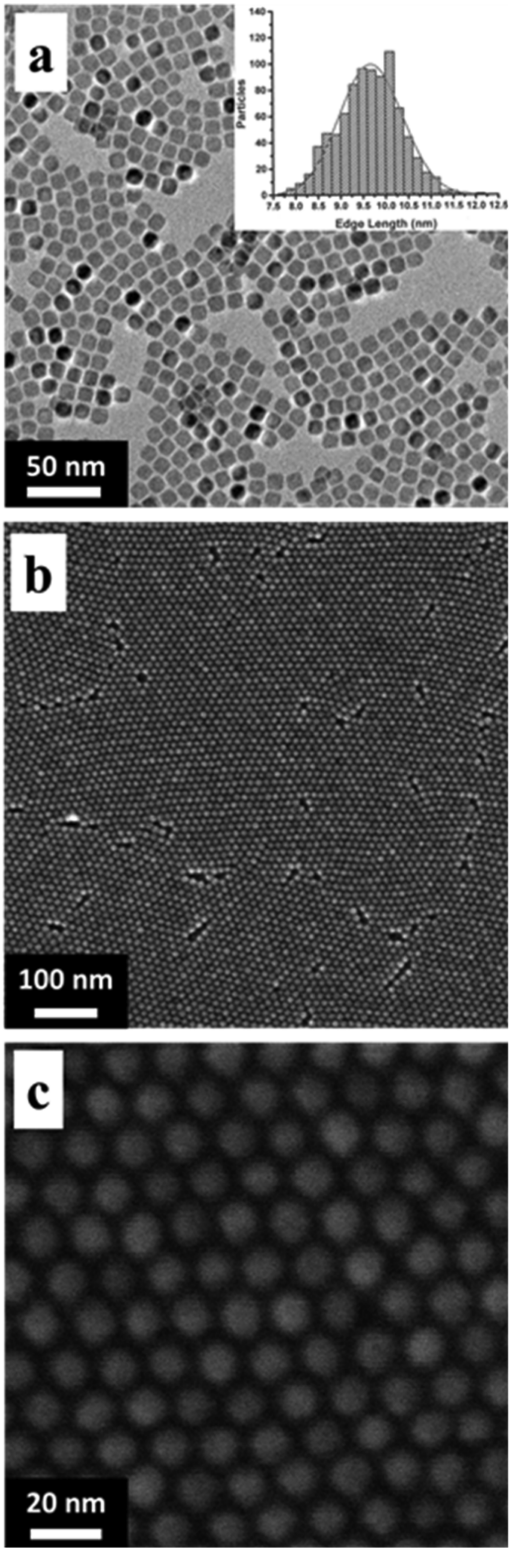

Figure 1. (a) TEM image of the as-synthesized, oleate-capped PbS NCs used in this study showing truncated cubic geometry Inset: histogram of edge lengths of 873 measured NCs fitted with a Gaussian curve (red line) used to determine average NC size (9.7 nm) and standard deviation (0.7 nm). (b) Self-assembled monolayer of same PbS NCs on Si/SiO_2 formed by casting a solution of NCs in hexanes onto an acetonitrile subphase. NCs self-assembly into locally ordered domains with void space defects along domain boundaries (c) Higher magnification of same film as in (b) showing the hexagonal close-packed structure of a single domain.

The dried PbS NC powder was dispersed in hexanes using sonication to form a 4 mg/mL colloidal suspension. 40 μL of this suspension was then delivered to the edge of a 25 mL round PTFE crucible holding 2 mL of dried acetonitrile. The NC/hexanes suspension was wicked around the circumference of the acetonitrile/PTFE and a NC monolayer spontaneously nucleated and grew from the opposite side to cover the entire acetonitrile subphase in approximately 10 s. Figures 1b,c show large-area monolayers formed when a solution of the as-synthesized, oleate-capped PbS NCs are cast on top of an acetonitrile subphase held in a PTFE crucible. The dried NC monolayer is a solid sheet held together primarily by the van der Waals interactions of their ligand shells.[17] While cubic PbS NCs have been reported as preferentially packing into cubic arrays,[18] the truncated edges of these quasi-cubic NCs produce hexagonally close-packed domains that range from 10 to 50 NCs across. The primary defects in these arrays are the void spaces that run along the boundaries between domains and the vacancy defects within a domain where a single NC is absent.

Figure 2a shows the method we used to perform ligand exchange (from oleate to one of the ligands in Table 1) of the freestanding NC monolayer at the liquid−air interface.[16] Stock solutions of all ligands were prepared in tetrahydrofuran at 3.89 M, except for the dicarboxylic acids, which were prepared at 3.89 mM; the lower concentration was necessary to prevent crystallization during film deposition. Following formation of the PbS NC monolayer on acetonitrile, 10 μL of the stock solution of the desired ligand was injected into the subphase via syringe; the concentration of ligand in the subphase was 19.4 μM for dicarboxylic acids and 19.4 mM for all other ligands. The PTFE dish was covered to prevent evaporation of the subphase, and the ligand exchange was allowed to proceed for 30 min under ambient atmosphere and temperature. The injected ligand displaces the native oleate ligands from the NC surface, which partitions into the acetonitrile subphase as oleic acid. During this time the film contracted as the particle spacing decreased; film contraction always stopped in less than 30 min (see the Supporting Information, Movie S1). We then pipetted off the subphase with a clean syringe to transfer the ligand-exchanged NC monolayer onto an underlying substrate for analysis. Transferred films were dried in a vacuum oven for 30 min at 70 °C and 25 in.Hg to remove residual solvent.

We compared the structures of films of PbS NCs following ligand exchange with both bridging and nonbridging carboxylic acid and thiol ligands of various lengths (Table 1). We employ the general term "bridging" for any bidentate ligand with the possibility to simultaneously coordinate two neighboring NC surfaces. Table 1 also lists the length of each ligand when coordinated to one Pb^{2+} ion; the expected interparticle spacing is twice this length for the limiting case of zero intercalation.

Near-infrared absorption spectroscopy of the films that underwent ligand exchange shows that (i) treatment with the carboxylic acids produces no change in the band edge absorption maximum, (ii) treatment with thiols produces a 10−13 nm bathochromic shift of the absorption with no increase in absorption line width (due to relaxation of exciton confinement by the thiolate),[19,20] and (iii) the position of the absorption maximum is invariant with ligand length (see Supporting Information, Figure S3). We conclude that the NCs are not being etched or sintered and that the electronic coupling between adjacent NCs does not perturb the exciton energy. Etching of the corners and edges of the NCs does occur if we allow the exchange to proceed for several hours.

DOI: 10.1021/acs.langmuir.6b01444
Langmuir 2016, 32, 6666−6673

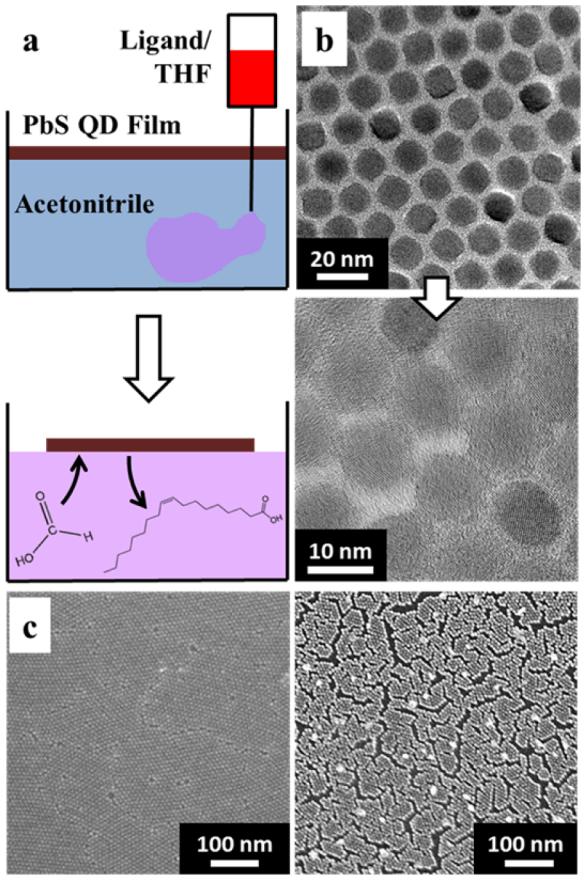

Figure 2. (a) Diagram of the interfacial ligand exchange process. Following assembly of an oleate-caped PbS NC monolayer on the acetonitrile subphase, a stock solution of the shorter ligand in tetrahydrofuran is injected into the subphase (top). The native oleate is displaced by the shorter ligand (shown here as formic acid, bottom). (b) TEM images of the PbS NC monolayer with the native oleate (top) and following exchange with formic acid (bottom, scale bar = 10 nm). (c) FE-SEM images of formic acid-exchanged films where the exchange was either performed on acetonitrile (left) or on a Si/SiO_2 substrate (right). The Si/SiO_2 substrate with the NC layer was submerged for 30 min in a 19.5 mM solution of formic acid in acetonitrile. Following exchange, we rinsed the film with acetonitrile and dried in a vacuum oven at 70 °C and 25 in.Hg pressure for 30 min.

pK_a of the Incoming Ligand Appears To Determine the Number of Oleate Ligands Displaced from the Film. We measured the concentration of oleate molecules displaced from the NC layer into the acetonitrile subphase by proton nuclear magnetic resonance (^{1}H NMR) spectroscopy of the subphase solution following the ligand exchange. This analysis was performed for the longest and shortest bridging and nonbridging ligands (for both carboxylic acids and thiols) because these ligands represent the limits of pK_a and solubility among the samples tested. Table 2 lists the measured concentrations of displaced oleate (which is present as oleic acid), which were determined by integration of the vinyl proton signal of oleic acid referenced to an internal biphenyl standard (see the Supporting Information for all NMR spectra). Measurable quantities of oleic acid only exist in the acetonitrile subphase once a new coordinating ligand is introduced; since oleic acid is readily soluble in acetonitrile, this observation implies that the native oleate ligand is covalently bound to the NCs in the monolayer.

The two monocarboxylic acids displace the same quantity of oleate, as do the four thiols (monoand disubstituted) analyzed. The monocarboxylic acids displace approximately 20% more oleate than the same concentration of the analogous thiols. Dicarboxylic acids are much less soluble in acetonitrile than monocarboxylic acids, and despite using a tetrahydrofuran cosolvent, the maximum concentration of dicarboxylic acids that we could add was 1000-fold lower than the added concentrations of other ligands. Despite the lower added concentration, the dicarboxylic acids still displaced nearly 50% as much oleate as did the monocarboxylic acids.

Oleic acid bound to the NC surface is coordinated to Pb^{2+} ions on the NC surface in its deprotonated oleate form.[21,22] Hens and co-workers have shown that the displacement of oleate by a carboxylic acid or thiol requires proton transfer from the incoming ligand to the oleate.[23] The lack of surface etching of our NCs upon ligand exchange, evident in either the TEM images or NIR absorbance spectra, suggests that most of the bound oleate leaves as oleic acid and not as a lead(II) oleate complex. On the basis of their respective octanol–water partition coefficients—log P = −0.54 for formic acid[24] and 1.27 for ethanethiol[25]—and on the respective binding affinities of thiolates and carboxylates to Pb^{2+}, we would expect thiols to more effectively permeate into the oleate ligand shell and displace oleate than carboxylic acids, but we observe the opposite. We attribute the carboxylic acids' higher yield of oleate displacement to their much lower pK_a values: 3.75 for formic acid compared to 10.61 for ethanethiol. The trend in oleate displacement rate with pK_a is also consistent with a previous report by Law and co-workers, who showed that oxalic acid (p$K_{a,1}$ = 1.25) displaces oleate more efficiently than formic acid (pK_a = 3.75) in drop-cast films of PbS quantum dots.[3]

Ligand Length Controls Interparticle Spacing within Ordered Domains. We used high-resolution TEM of the ligand-exchanged films (Figure 2b) to determine the average spacing between nearest neighbors within ordered domains of PbS NCs; Table 2 summarizes these measurements. The average surface-to-surface separation (interfacial spacing) decreases following ligand exchange for all samples. Comparison between the molecular length of the ligands in Table 1 and the measured interfacial spacing shows that except for formic acid, which does not intercalate, nonbridging ligands intercalate by 25–40% (meaning that the measured length is 60–75% of twice the ligand length); intercalation stabilizes the NC array through van der Waals interactions.[26] In contrast, the bridging carboxylate and thiolate ligands all exhibit interfacial spacings that are very close to the lengths of their lead(II) complexes. This result suggests that the disubstituted ligands form rigid bridges between the NCs and can be used to control nearest-neighbor spacing within NC domains.

Figure 2c shows the structures of two PbS NC monolayers treated with formic acid: one formed by ligand exchange at the liquid–air interface (left) and one formed by ligand exchange within a monolayer that was predeposited on an Si/SiO_2 wafer and then soaked in a solution of formic acid in acetonitrile. The inability of NCs to reorganize on the Si/SiO_2 substrate produces large cracks in the solid state exchange; small domains are able to pack together, but the film is unable to contract over longer distances as it does when floating on a liquid subphase.

Rate of Ligand Exchange Influences the Final Packing Structure of the Film. Figure 3 shows plots of the particle density within monolayers of PbS NCs after treatment with each thiol or carboxylic acid ligand at the liquid–air interface.

DOI: 10.1021/acs.langmuir.6b01444
Langmuir 2016, 32, 6666–6673

Table 1. Structures, pK_a Values, and Lengths of Ligands for PbS NCs within Monolayers

	structure	pK_a[a]	length[b] (nm)	structure	pK_a	length[b] (nm)
nonbridging	H−COOH	3.7[c]	0.40	CH_3CH_2−SH	10.61[d]	0.58
	CH_3−COOH	4.76[c]	0.48	$CH_3(CH_2)_2$−SH	10.7[e]	0.70
	CH_3CH_2−COOH	4.87[c]	0.62	$CH_3(CH_2)_3$−SH	11.51[d]	0.83
	$CH_3(CH_2)_2$−COOH	4.83[c]	0.77	$CH_3(CH_2)_4$−SH	10.51[f]	0.96
	$CH_3(CH_2)_3$−COOH	4.83[c]	0.91	$CH_3(CH_2)_5$−SH	10.66[g]	1.08
	$CH_3(CH_2)_4$−COOH	4.85[c]	1.06			
	$CH_3(CH_2)_7C{=}C(CH_2)_7COOH$	9.85[h]	2.60			
bridging	HOOC−COOH	1.25, 3.81[c]	0.73	HS−$(CH_2)_3$−SH	9.86[f]	0.97
	HOOC−$(CH_2)_2$−COOH	4.21, 5.64[c]	0.94	HS−$(CH_2)_4$−SH	10.07[f]	1.10
	HOOC−$(CH_2)_4$−COOH	4.41, 5.41[c]	1.14	HS−$(CH_2)_6$−SH	10.17[f]	1.35
	HOOC-$(CH_2)_6$-COOH	4.52[c]	1.35	HS−$(CH_2)_8$−SH	10.19[f]	1.60
	HOOC−$(CH_2)_8$−COOH	4.59, 5.59[c]	1.56			
	HOOC−$(CH_2)_{10}$−COOH	4.48[f]	1.76			

[a]Where two values are listed these indicate the dissociation constants for the first and second deprotonation. [b]Calculated for the extended geometry of Pb^{2+}−OOC−R for the nonbridging carboxylate, Pb^{2+}−S−R for the nonbridging thiolate, Pb^{2+}−OOC−R−OOC−Pb^{2+} for the bridging carboxylate, or Pb^{2+}−S−R−S−Pb^{2+} for the bridging thiolate, see the Supporting Information for details. [c]Reference 27. [d]Reference 28. [e]Reference 29. [f]Values calculated by the CAS Registry using Advanced Chemistry Development Software. [g]Reference 30. [h]Reference 31.

Table 2. Summary of Displaced Oleate Concentrations and Structural Parameters for the PbS NC Monolayers

	displaced oleate concn; ^{1}H NMR (μM)	edge-to-edge separation (within ordered domains); HR-TEM (nm)	center-to-center distance (av over 10 mm^2); GISAXS (nm)
$CH_3(CH_2)_7C{=}C(CH_2)_7COOH$ (native oleate)	n/a	3.1 ± 0.5	14.2 ± 0.3
H−COOH	27	0.9 ± 0.1	13.4 ± 0.3
$CH_3(CH_2)_4$−COOH	27	1.5 ± 0.3	13.6 ± 0.3
HOOC−COOH[b]	12	0.7 ± 0.1	14.1 ± 0.3
HOOC−$(CH_2)_{10}$−COOH[b]	14	1.8 ± 0.3	13.7 ± 0.3
CH_3CH_2−SH	21	0.7 ± 0.2	not measured
$CH_3(CH_2)_5$−SH	22	1.5 ± 0.3	not measured
HS−$(CH_2)_3$−SH	21	1.0 ± 0.2	not measured
HS−$(CH_2)_8$−SH	21	1.6 ± 0.3	not measured

[a]All error bars represent standard deviations of multiple measurements. [b]The added concentration was 19.4 μM for dicarboxylic acids and 19.4 mM for all other ligands due to the low solubility of dicarboxylic acids in acetonitrile.

We determined packing density by counting the number of NCs in 500 × 500 nm regions of the FE-SEM images of two to three separately prepared samples, at three separate locations within each sample. These regions contain many ordered domains separated by grain boundary-like defects. All ligands tested increase the particle density compared to the as-deposited monolayer coated with native oleate (Figure 3, orange dotted line); this result is corroborated by grazing-incidence small-angle X-ray scattering (GISAXS) measurements, which yield nearest-neighbor interparticle distances averaged over the entire film for four separately prepared samples (Table 2).

The in-plane Bragg diffraction peaks from GISAXS, shown in Figure 4 for native oleate case, occur at in-plane scattering vector modulus values of $q_{xy} \approx 0.51 \pm 0.02$, 0.90 ± 0.02, and 1.02 ± 0.02 nm^{-1}. These are closely matched to the first three allowed $\{hk\}$ diffraction peaks ($\{10\}$, $\{11\}$, and $\{20\}$) for a hexagonal 2D crystal where $q_{xy} = 2\pi(h^2 + k^2 + hk)^{1/2}(2/\sqrt{3})\,a^{-1}$ with lattice constant $a = 14.2 \pm 0.3$ nm. Other groups have reported 3D bulk assemblies of PbS NCs with a FCC lattice.[32,33]

The purple dotted line in Figure 3 corresponds to the particle density within a film NCs that was treated with formic acid after depositing it on a Si/SiO_2 wafer; this method of ligand exchange does not yield an increased packing density, when averaged over a 500 × 500 nm region. The highest packing efficiencies—26% higher than films of oleate-coated NCs—are in ethanethiol-treated films. We never observe the quadratic increase in packing density with decreasing ligand length expected from varying the interparticle spacing within a close-packed array of NCs. For instance, given the intradomain interparticle spacing for the ethanethiol-treated film listed in Table 2, the upper limit for particle density in this film is 50% higher than the density of the oleate film. We do not achieve this upper limit due to void space between well-ordered domains. These voids are apparent in the SEM images of all the ligand-exchanged NC monolayers (Figures S6−S9 in the Supporting Information).

Figure 3 shows that the density of NCs increases as ligand length decreases for thiols (b), but not for carboxylic acids (a), despite the fact that short and long carboxylic acids displace the same amount of oleate (Table 2). For monocarboxylic acids (red squares, Figure 3a), a maximum in NC packing efficiency is observed for propionic acid-treated films. We propose that the decrease in particle density with decreasing ligand length for the shortest monocarboxylic acids is due to trapping of films treated with these ligands in "kinetic" structures with higher defect densities. As the ligand length decreases, the pK_a of the acid decreases; the lower the pK_a, the faster the proton exchange process with oleate and the faster the ligand exchange and contraction of the film (see the Supporting Information). Changes in the rate of oleate displacement with ligand pK_a would also explain why ethanethiol-treated NCs pack more densely than formic acid-treated NCs even though the carboxylic acid displaces more oleate; the higher pK_a of the thiols probably displaces oleate at a slower rate and allows more time for NCs to rearrange into a close-packed configuration.

Bridging Ligands Enable Close-Packing within Ordered Domains at the Expense of Longer-Range Order. The particle density of films treated with dithiols or dicarboxylic acids is only weakly dependent, if dependent at

DOI: 10.1021/acs.langmuir.6b01444
Langmuir 2016, 32, 6666−6673

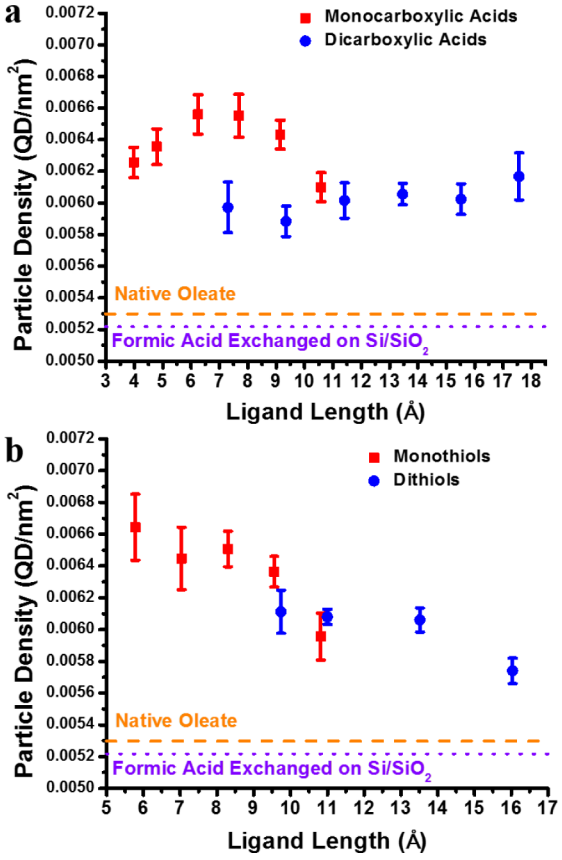

Figure 3. Plots of the average particle density measured by FE-SEM in PbS NC monolayers following exchange with nonbridging (red squares) and bridging (blue circles) ligands containing either (a) carboxylate or (b) thiolate binding groups as a function of ligand length. Values for monolayers with the native oleate (orange dashed line) or exchanged with formic acid on an Si/SiO_2 substrate (purple dotted line) are plotted for comparison. All samples ligand-exchanged at the liquid–air interface show higher packing densities than the oleate-capped NC samples or the sample exchanged on the solid substrate. The NC density was determined by counting the number of NCs within three 500 × 500 nm regions within each of two-to-three separately prepared samples. Reported values are averages (and standard deviations) of these six-to-nine measurements. These standard deviations are largely the result of film-to-film variation in particle density; spot-to-spot variations in particle densities within any single film were <1%.

all, on ligand length; for instance, treatment with dodecanedioic acid (HOOC–$(CH_2)_{10}$–COOH, the longest diacid in Figure 3a) produces similar particle densities as treatment with oxalic acid (HOOC–COOH, the shortest diacid in Figure 3a), and center-to-center NC distance from GISAXS measurements show that treatment with dodecanedioic acid actually produces smaller nearest-neighbor spacing than treatment with oxalic acid, when averaged over the whole film. Figure 5 compares, visually, the packing structures formed by the bridging ligands oxalic acid, dodecanedioic acid, 1,3-propanedithiol, and 1,8-octanedithiol explain this behavior. The shorter bridging ligands form smaller NC domains with larger interdomain gaps than the longer bridging ligands. Even within what appear to be single NC domains, oxalic acid forms local clusters of NCs separated by small cracks (Figure 5e).

We believe that despite the well-defined interparticle distance within ordered domains enabled by bridging ligands, the particle density depends only weakly on the length of bridging ligands because NCs joined by bridging ligands are less able to reorganize to a close-packed structure. The fine control over interparticle spacing achieved by bridging ligands within small domains comes at the cost of structural order at longer length scales.

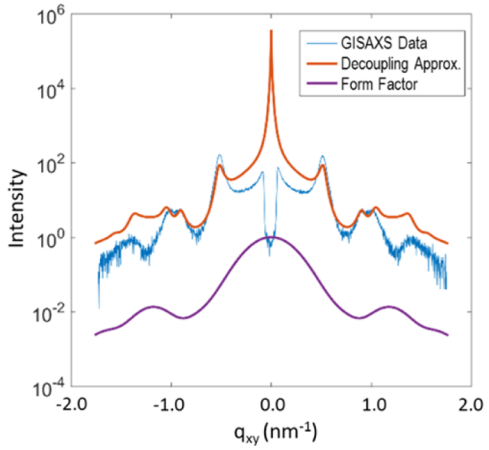

Figure 4. GISAXS data and analysis for NCs coated with native oleate. The q_{xy} dependence of the in-plane scattered intensity data (blue) was produced by integrating the 2D scattering pattern (Figure S5) over an out-of-plane scattering vector range from q_z = 0.25 to 0.35 nm^{-1}. The normalized form factor (purple) describes the scattered intensity contribution from one ensemble-averaged particle. A simulation of the scattering using the decoupling approximation (orange) to model the influence of NC polydispersity influences on overall film structure described as described in the Supporting Information.

Line shape analysis of the data in Figure 4 provides further insight into the nature of the disorder in the carboxylic acid-treated systems. Williamson–Hall peak-shape analysis[34] (eq S4 in the Supporting Information) includes contributions to line broadening from both domain size effects and strain broadening effects. Employing this equation to analyze the GISAXS data from the NC systems reveals that the domain size is in excess of 10 NCs across for all samples and responsible for less than 1/4 of the total peak broadening of the Bragg diffraction peaks. This result indicates that strain, due to deviation of the NCs from their ideal lattice positions in response to defects within the film (or "apparent strain", as defined by Stokes and Wilson[35]), is the dominant mechanism for the peak broadening in the NC films. The apparent strain (here, measured along the {10} direction) ranges from 0.06 to 0.08 in all ligand-exchanged samples.

Our combined data suggest the following sources of disorder in the NC array. Rapid ligand exchange can result in NCs' becoming kinetically trapped in frustrated packing geometries, which may include the relative rotation of NCs or the formation of grain boundaries. Bridging ligands can create stable configurations where isolated clusters of NCs are held together by covalent linkages. Reorganization of these clusters into close-packed arrays is gated by the energy to deform these bridging ligands. The apparent strain observed through GISAXS indicates local defects have a substantial long-range impact on lattice packing. Further work should be explored to understand the specific energetic barriers to reorganization for both types of defects and how these defects can be removed through either control of the ligand exchange conditions or chemical treatment of the films following ligand exchange.

DOI: 10.1021/acs.langmuir.6b01444
Langmuir 2016, 32, 6666–6673

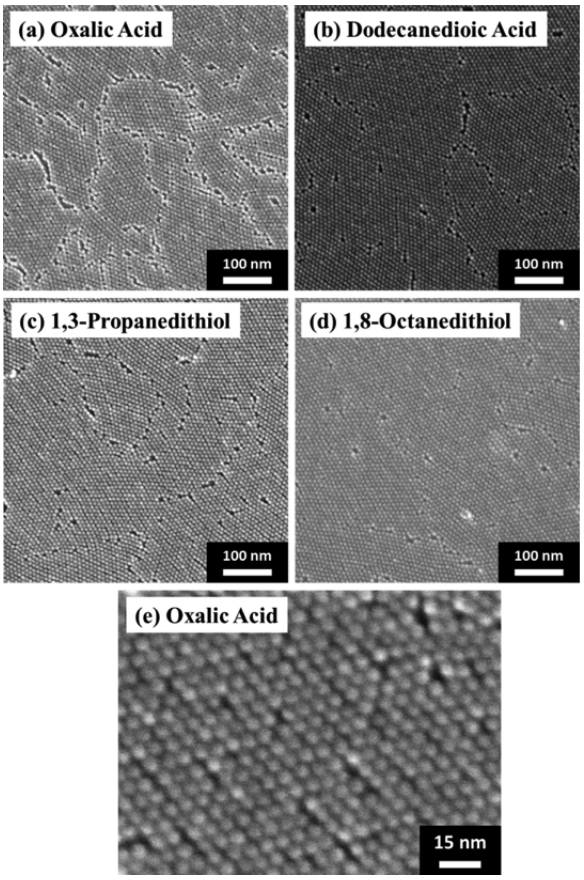

Figure 5. FE-SEM images of the PbS NC monolayers exchanged with the shortest (left) and longest (right) bridging carboxylic acids (a, b) and thiols (c, d) examined (scale bars = 100 nm). Films exchanged with shorter bridging ligands have more and larger interdomain gaps than films exchanged with longer bridging ligands. This effect limits the particle density achievable upon exchange with the shorter bridging ligands. (e) Higher magnification image of an oxalic acid-exchanged PbS NC monolayer showing small gaps between ordered domains characteristic of films exchanged with a short bridging ligand.

CONCLUSIONS

We prepared compact monolayers of PbS NCs using a range of mono- and dicarboxylic acids and mono- and dithiols by exchanging the native ligand, oleate, for these ligands on a free-standing NC monolayer floating on an acetonitrile subphase. The average interparticle spacing decreased upon ligand exchange for all samples, which could be tracked through the visible contraction of the film. HR-TEM showed that dicarboxylic acids and thiols adopt a bridging geometry between adjacent NCs and allow for well-controlled nearest-neighbor separation. Monocarboxylic acids and thiols both adopt intercalated structures, with the exception of formic acid. Carboxylic acids more effectively displace oleates than do thiols, which we attribute to the lower pK_a values of carboxylic acids. The fast exchange kinetics of the films upon treatment with short carboxylic acids kinetically trap the NCs into frustrated packing geometries and lead to a nonmonotonic dependence of particle density on ligand length. The highest particle densities for carboxylic acid-treated monolayers were achieved with propionic acid. The slower exchange kinetics in the case of thiols led to a monotonic dependence of particle density on ligand length. Ordering of the NCs bridged by disubstituted ligands appears to be limited by the flexibility of the bridging ligand. The fine control over nearest-neighbor separation afforded by bridging ligands therefore inevitably comes at the cost of poorer packing over longer distances.

ASSOCIATED CONTENT

Supporting Information

The Supporting Information is available free of charge on the ACS Publications website at DOI: 10.1021/acs.langmuir.6b01444.

Additional TEM and FE-SEM images and absorbance spectra, calculations of ligand length, discussion of particle stability, GISAXS raw data and model description, and Figures S1−S9 (PDF)

Videos of film formation and exchange (ZIP)

AUTHOR INFORMATION

Corresponding Author

*E-mail: e-weiss@northwestern.edu (E.A.W.).

Notes

The authors declare no competing financial interest.

ACKNOWLEDGMENTS

This project was funded by the National Science Foundation through the Northwestern Materials Research Science and Engineering Center (Grant DMR-1121262). Electron microscopy studies were performed using the NU*ANCE* facilities of Northwestern University. The NU*ANCE* Center is supported by the International Institute for Nanotechnology, the MRSEC (NSF DMR-1121262), the Keck Foundation, the State of Illinois, and Northwestern University. The X-ray Diffraction Facility is supported by the MRSEC. The authors also acknowledge Northwestern University's Integrated Molecular Structure Education and Research Center (IMSERC) facilities for the use of the AVANCE III 500 MHz NMR spectrometer.

REFERENCES

(1) Klem, E. J. D.; Shukla, H.; Hinds, S.; MacNeil, D. D.; Levina, L.; Sargent, E. H. Impact of dithiol treatment and air annealing on the conductivity, mobility, and hole density in PbS colloidal quantum dot solids. *Appl. Phys. Lett.* **2008**, *92*, 212105/1−21205/3.

(2) Dong, A.; Jiao, Y.; Milliron, D. J. Electronically Coupled Nanocrystal Superlattice Films by in Situ Ligand Exchange at the Liquid-Air Interface. *ACS Nano* **2014**, *7*, 10978−10984.

(3) Zarghami, M. H.; Liu, Y.; Gibbs, M.; Gebremichael, E.; Webster, C.; Law, M. p-Type PbSe and PbS Quantum Dot Solids Prepared with Short-Chain Acids and Diacids. *ACS Nano* **2010**, *4*, 2475−2485.

(4) Koh, W.-k.; Saudari, S. R.; Fafarman, A. T.; Kagan, C. R.; Murray, C. B. Thiocyanate-Capped PbS Nanocubes: Ambipolar Transport Enables Quantum Dot Based Circuits on a Flexible Substrate. *Nano Lett.* **2011**, *11*, 4764−4767.

(5) Tang, J.; Kemp, K. W.; Hoogland, S.; Jeong, K. S.; Liu, H.; Levina, L.; Furukawa, M.; Wang, X.; Debnath, R.; Cha, D.; Chou, K. W.; Fischer, A.; Amassian, A.; Asbury, J. B.; Sargent, E. H. Colloidal-quantum-dot photovoltaics using atomic-ligand passivation. *Nat. Mater.* **2011**, *10*, 765−771.

(6) Yakunin, S.; Dirin, D. N.; Protesescu, L.; Sytnyk, M.; Tollabimazraehno, S.; Humer, M.; Hackl, F.; Fromherz, T.; Bodnarchuk, M. I.; Kovalenko, M. V.; Heiss, W. High Infrared Photoconductivity in Films of Arsenic-Sulfide-Encapsulated Lead-Sulfide Nanocrystals. *ACS Nano* **2014**, *8*, 12883−12894.

(7) Talapin, D. V.; Murray, C. B. PbSe Nanocrystal Solids for n- and p-Channel Thin Film Field-Effect Transistors. *Science* **2005**, *310*, 86−89.

DOI: 10.1021/acs.langmuir.6b01444
Langmuir 2016, 32, 6666−6673

(8) Liu, Y.; Gibbs, M.; Puthussery, J.; Gaik, S.; Ihly, R.; Hillhouse, H. W.; Law, M. Dependence of Carrier Mobility on Nanocrystal Size and Ligand Length in PbSe Nanocrystal Solids. *Nano Lett.* **2010**, *10*, 1960−1969.
(9) Boehme, S. C.; Walvis, T. A.; Infante, I.; Grozema, F. C.; Vanmaekelbergh, D.; Siebbeles, L. D. A.; Houtepen, A. J. Electrochemical Control over Photoinduced Electron Transfer and Trapping in CdSe-CdTe Quantum-Dot Solids. *ACS Nano* **2014**, *8*, 7067−7077.
(10) Zhang, J.; Tolentino, J.; Smith, E. R.; Zhang, J.; Beard, M. C.; Nozik, A. J.; Law, M.; Johnson, J. C. Carrier Transport in PbS and PbSe QD Films Measured by Photoluminescence Quenching. *J. Phys. Chem. C* **2014**, *118*, 16228−16235.
(11) Weidman, M. C.; Yager, K. G.; Tisdale, W. A. Interparticle Spacing and Structural Ordering in Superlattice PbS Nanocrystal Solids Undergoing Ligand Exchange. *Chem. Mater.* **2014**, *27*, 474−482.
(12) Gao, J.; Zhang, J.; van de Lagemaat, J.; Johnson, J. C.; Beard, M. C. Charge Generation in PbS Quantum Dot Solar Cells Characterized by Temperature-Dependent Steady-State Photoluminescence. *ACS Nano* **2014**, *8*, 12814−12825.
(13) Bhaumik, S.; Pal, A. J. Quantum Dot Light-Emitting Diodes in the Visible Region: Energy Level of Ligands and Their Role in Controlling Interdot Spacing and Device Performance. *J. Phys. Chem. C* **2013**, *117*, 25390−25396.
(14) Li, H.; Chen, D.; Li, L.; Tang, F.; Zhang, L.; Ren, J. Size- and Shape-controlled Synthesis of PbSe and PbS Nanocrystals via a Facile Method. *CrystEngComm* **2009**, *12*, 1127−1133.
(15) Wise, F. W. Lead Salt Quantum Dots: the Limit of Strong Quantum Confinement. *Acc. Chem. Res.* **2000**, *33*, 773−780.
(16) Dong, A.; Chen, J.; Oh, S. J.; Koh, W.-k.; Xiu, F.; Ye, X.; Ko, D.-K.; Wang, K. L.; Kagan, C. R.; Murray, C. B. Multiscale Periodic Assembly of Striped Nanocrystal Superlattice Films on a Liquid Surface. *Nano Lett.* **2011**, *11*, 841−846.
(17) He, J.; Kanjanaboos, P.; Frazer, N. L.; Weis, A.; Lin, X.-M.; Jaeger, H. M. Fabrication and Mechanical Properties of Large-Scale Freestanding Nanoparticle Membranes. *Small* **2010**, *6*, 1449−1456.
(18) Yamamuro, S.; Sumiyama, K. Why do cubic nanoparticles favor a square array? Mechanism of shape-dependent arrangement in nanocube self-assemblies. *Chem. Phys. Lett.* **2006**, *418*, 166−169.
(19) Malicki, M.; Knowles, K. E.; Weiss, E. A. Gating of hole transfer from photoexcited PbS quantum dots to aminoferrocene by the ligand shell of the dots. *Chem. Commun.* **2013**, *49*, 4400−4402.
(20) Amin, V. A.; Aruda, K. O.; Lau, B.; Rasmussen, A. M.; Edme, K.; Weiss, E. A. The Dependence of the Bandgap of CdSe Quantum Dots on the Surface Coverage and Bidning Mode of an Exciton-Delocalizing Ligand, Methylthiophenolate. *J. Phys. Chem. C* **2015**, *119*, 19423−19429.
(21) Lobo, A.; Möller, T.; Nagel, M.; Borchert, H.; Hickey, S. G.; Weller, H. Photoelectron Spectroscopic Investigations of Chemical Bonding in Organically Stabilized PbS Nanocrystals. *J. Phys. Chem. B* **2005**, *109*, 17422−17428.
(22) Cass, L. C.; Malicki, M.; Weiss, E. A. The Chemical Environments of Oleate Species within Samples of Oleate-Coated PbS Quantum Dots. *Anal. Chem.* **2013**, *85*, 6974−6979.
(23) Fritzinger, B.; Capek, R. K.; Lambert, K.; Martins, J. C.; Hens, Z. Utilizing Self-Exchange To Address the Binding of Carboxylic Acid Ligands to CdSe Quantum Dots. *J. Am. Chem. Soc.* **2010**, *132*, 10195−10201.
(24) Verliefde, A. R. D.; Cornelissen, E. R.; Heijman, S. G. J.; Verberk, J. Q. J. C.; Amy, G. L.; Van der Bruggen, B.; van Dijk, J. C. The role of electrostatic interactions on the rejection of organic solutes in aqueous solutions with nanofiltration. *J. Membr. Sci.* **2008**, *322*, 52−66.
(25) Leclercq, S.; Reineccius, G. A.; Milo, C. Model Studies on the Influence of Matrix Type and Storage Environment on the Stability of a Model Aroma Mixture during Storage. *J. Agric. Food Chem.* **2007**, *55*, 421−425.
(26) Gattas-Asfura, K. M.; Constantine, C. A.; Lynn, M. J.; Thimann, D. A.; Ji, X.; Leblanc, R. M. Characterization and 2D Self-Assembly of CdSe Quantum Dots at the Air-Water Interface. *J. Am. Chem. Soc.* **2005**, *127*, 14640−14646.
(27) *CRC Handbook of Chemistry and Physics*, 95th ed.; CRC Press: 2015; www.hbcpnetbase.com (accessed May 16, 2015).
(28) Danehy, J. P.; Parameswaran, K. N. Acidic Dissociation Constants of Thiols. *J. Chem. Eng. Data* **1968**, *13*, 386−389.
(29) Kelly, C. P.; Cramer, C. J.; Truhlar, D. G. Adding Explicit Solvent Molecules to Continuum Solvent Calculations for the Calculation of Aqueous Acid Dissociation Constants. *J. Phys. Chem. A* **2006**, *110*, 2493−2499.
(30) Chan, J. W.; Hoyle, C. E.; Lowe, A. B.; Bowman, M. Nucleophile-Initiated Thiol-Michael Reactions: Effect of Organocatalyst, Thiol, and Ene. *Macromolecules* **2010**, *43*, 6381−6388.
(31) Kanicky, J. R.; Shah, D. O. Effect of Degree, Type, and Position of Unsaturation on the pKa of Long-Chain Fatty Acids. *J. Colloid Interface Sci.* **2002**, *256*, 201−207.
(32) Li, R.; Bian, K.; Hanrath, T.; Bassett, W. A.; Wang, Z. Decoding the Superlattice and Interface Structure of Truncated PbS Nanocrystal-assembled Supercrystal and Associated Interaction Forces. *J. Am. Chem. Soc.* **2014**, *136*, 12047−55.
(33) Quan, Z.; Loc, W. S.; Lin, C.; Luo, Z.; Yang, K.; Wang, Y.; Wang, H.; Wang, Z.; Fang, J. Tilted Face-centered-cubic Supercrystals of PbS Nanocubes. *Nano Lett.* **2012**, *12*, 4409−4413.
(34) Williamson, G.; Hall, W. X-ray Line Broadening from Filed Aluminium and Wolfram. *Acta Metall.* **1953**, *1*, 22−31.
(35) Stokes, A. R.; Wilson, A. J. C. The Diffraction of X-Rays By Distorted Crystal Aggregates. *Proc. Phys. Soc.* **1943**, *56*, 174.

DOI: 10.1021/acs.langmuir.6b01444
Langmuir 2016, 32, 6666−6673